Defect Structure of Ni,Co-Doped $LiNbO_3$ and $LiTaO_3$

Marcus Paul,*,† Mitsuharu Tabuchi,*,‡ and Anthony R. West*,†

Department of Chemistry, University of Aberdeen, Meston Walk, Aberdeen AB24 3UE, Scotland, and Osaka National Research Institute, Midorigaoka 1-8-31, Ikeda, Osaka 563, Japan

Received July 17, 1997[⊗]

The stoichiometries and structures of $LiNbO_3$ and $LiTaO_3$ doped with Ni^{2+} and Co^{2+} have been established through a combination of phase diagram determination, Rietveld refinement of powder X-ray diffraction data, extended X-ray absorption fine structure spectroscopy on the Ni, Co K edges, and magnetic measurements. Extensive ranges of Ni^{2+},Co^{2+}-containing solid solutions form by the principal substitution mechanism 3Li + Nb,Ta ⇌ 4Ni,Co. A secondary substitution mechanism, observed with both doped and undoped $LiNbO_3$ and $LiTaO_3$ is 5Li ⇌ Nb, Ta. All results are consistent with substitution of Ni^{2+},Co^{2+} onto primarily the Li sites but sometimes, depending on composition, also onto Nb/Ta sites; in both cases, the sites have off-center, distorted octahedral coordination. The doped compositions can be divided into two regions: first, region II in which the Nb/Ta sites are full but Li sites contain a random mixture of Li, Ni/Co, Nb/Ta, and vacancies; these have the general formula [Li, Ni/Co, Nb/Ta, □][Nb/Ta]O_3 where □ is a cation vacancy. Second, region I in which there is insufficient Nb/Ta to fully occupy their own sites, the balance is made up of Ni/Co and the Li sites contain Li, Ni/Co, and vacancies, i.e., [Li, Ni/Co, □][Nb/Ta, Ni/Co]O_3. Regions I and II are separated by a line of constant Nb/Ta content in which the substitution mechanism 2Li ⇌ Ni, Co occurs. On this line, Nb/Ta sites are fully occupied and Li sites contain a mixture of Li, Ni/Co, and vacancies. Magnetic measurements support the valency of both dopants (Co^{2+} and Ni^{2+} in high-spin state) and show the presence of weak magnetic coupling between these dopants at 4 K.

Introduction

Lithium niobate, $LiNbO_3$, and lithium tantalate, $LiTaO_3$, are important ferroelectric materials exhibiting a wide range of physical properties which are of technological interest. These materials are used in numerous electrical and optical devices with applications as electrooptic light modulators, holographic storage devices, thermal detectors, and filters in communication circuits.[1] The physical properties depend on the defects in the structure and can be improved by doping with other cations.

$LiNbO_3$ and $LiTaO_3$ have the same crystal structure which belongs to the rhombohedral (trigonal) space group $R3c$.[2,3] The structure consists of approximately hexagonal close-packed oxide ions where two-thirds of the octahedral sites are occupied by cations: the cations are stacked in such a manner that the sequence Li^+, Nb^{5+}/Ta^{5+}, and cation vacancy repeats every third layer, as shown in Figure 1*a*. Ferroelectric behavior arises when Li^+ and Nb^{5+}/Ta^{5+} are displaced from their octahedral centers in opposite directions along the *c*-axis toward adjacent empty octahedra, Figure 1a.

$LiNbO_3$ and $LiTaO_3$ are nonstoichiometric phases with variable compositions that extend from the stoichiometric composition to a Li deficiency of several mole percent, depending on temperature.[4] For both $LiNbO_3$ and $LiTaO_3$, the solid solution range extends from ∼44 to 50 mol % Li_2O at elevated temperatures but is much narrower at lower temperatures. $LiNbO_3$ melts congruently at composition ∼48.5% Li_2O:51.5% Nb_2O_5,[5] but this composition is metastable at room temperature and decomposes into $LiNbO_3$ and $LiNb_3O_8$ below ∼900 °C. Hereafter, $LiNbO_3$ with the ratio Li/(Li + Nb) = 0.50 is referred to as *stoichiometric LiNbO*$_3$, whereas the congruently melting composition with the ratio Li/(Li + Nb) = 0.485 is referred to as *congruent LiNbO*$_3$. This is also applicable to $LiTaO_3$, although in congruent $LiTaO_3$, probably Li/(Li + Ta) ≤ 0.485.[6] The nonstoichiometry arises from the mechanism $5Li^+ \rightleftharpoons Nb^{5+}/Ta^{5+}$ which creates cation vacancies according to the general formula $Li_{1-5x}(Nb/Ta)_{1+x}□_{4x}O_3$, where □ denotes a vacancy. There has been controversy over the sites in which these vacancies are accommodated but it is now generally accepted that they are created on the Li site.[7−9] Hence, the substitution mechanism may be written more fully as $[Li_{1-5x}(Nb/Ta)_x□_{4x}][(Nb/Ta)]O_3$.

† University of Aberdeen.
‡ Osaka National Research Institute.
[⊗] Abstract published in *Advance ACS Abstracts,* October 15, 1997.

(1) Townsend, P. D. *Adv. Solid State Chem.* **1993**, *3*, 271−285.
(2) Abrahams, S. C.; Reddy, J. M.; Bernstein, J. L. *J. Phys. Chem. Solids* **1966**, *27*, 997−1012.
(3) Abrahams, S. C.; Bernstein, L. J. *J. Phys. Chem. Solids* **1967**, *28*, 1685−1692.
(4) Roth, R. S.; Parker, H. S.; Brower, W. S.; Waring, J. L. In *Fast ion transport in solids: solid-state batteries and devices*; Van Gool, W., Ed.; North-Holland: Amsterdam, 1973; pp 217−232.
(5) Svaasand, L. O.; Eriksrud, M.; Nakken, G.; Grande, A. P. *J. Cryst. Growth* **1974**, *22*, 230−232.
(6) Bordui, P. F.; Norwood, R. G.; Bird, C. D.; Carella, J. T. *J. Appl. Phys.* **1995**, *78*, 4647−4650.
(7) Iyi, N.; Kitamura, K.; Izumi, F.; Yamamoto, J. K.; Hayashi, T.; Asano, H.; Kimura, S. *J. Solid State Chem.* **1992**, *101*, 340−352.
(8) Zotov, N.; Boysen, H.; Frey, F.; Metzger, T.; Born, E. *J. Phys. Chem. Solids* **1994**, *55*, 145−152.
(9) Wilkinson, A. P.; Cheetham, A. K.; Jarman, R. H. *J. Appl. Phys.* **1993**, *74*, 3080−3083.

S0897-4756(97)00511-5 CCC: $14.00

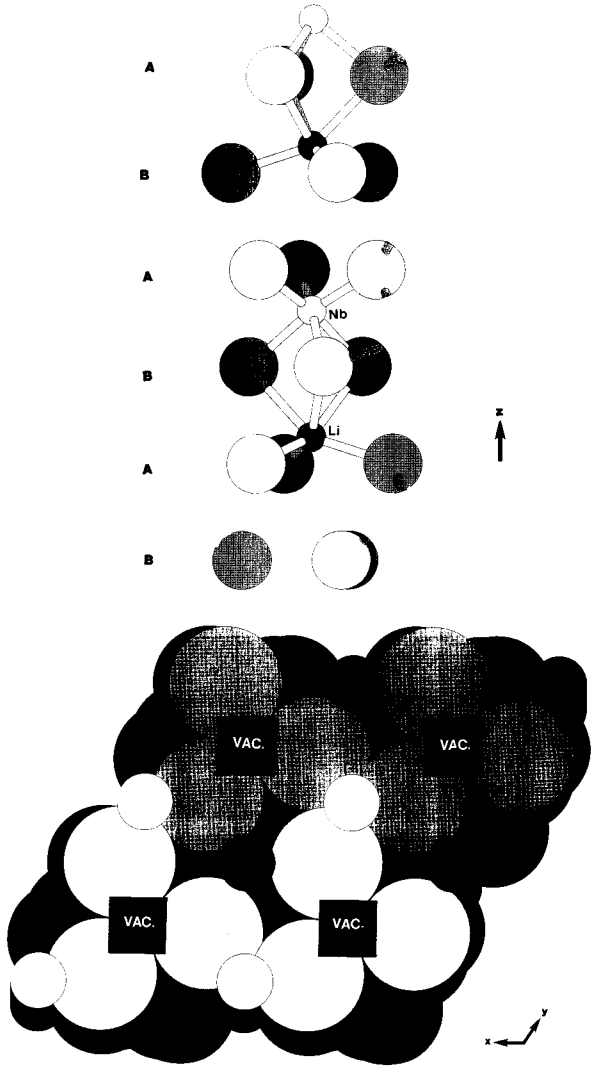

Figure 1. Crystal structure of $LiNbO_3$: (a, top) a column of face-sharing octahedra in the sequence: Nb, Li, vacancy; (b, bottom) close-packed oxide layers in projection with an Li site, small white circle, surrounded by three Nb sites and three octahedral vacancies in a coplanar arrangement.

$LiNbO_3$ and $LiTaO_3$ can be doped with a wide range of cations but the mechanism(s) of doping are not well established despite a very large number of studies using a wide range of techniques. Dopants are variously reported to be located on Li sites, Nb/Ta sites, and a mixture of the two and to occupy coordination polyhedra that are either distorted octahedra or regular octahedra. Part of the reason for the confusion arises because different strategies to doping are adopted. Some commence with stoichiometric $Li(Nb/Ta)O_3$, others with congruent $Li(Nb/Ta)O_3$. Some simply add the dopant as an oxide to the undoped material; others consider possible doping mechanisms and partially substitute the dopant cation for Li and/or Nb,Ta. Very often, a single doped composition is prepared and then various spectroscopic techniques are applied to deduce the defect structure.

Our approach follows earlier phase diagram studies which showed that $LiNbO_3$ and $LiTaO_3$ are generally very versatile host structures toward dopants and that extensive solid solution areas often form. In all cases studied so far, in the principal doping mechanism, the total number of cations remains constant, e.g. Li + 3Nb $\rightleftharpoons$ 4Ti for doping with Ti^{4+} ions.[10] These phase diagram studies have not been combined with structural studies, however, and consequently the defect mechanisms can only be speculated upon. Here, we report a multitechnique approach to resolve the doping mechanisms and defect structures in $LiNbO_3$ and $LiTaO_3$ doped with Ni^{2+} and Co^{2+}. This used a combination of phase diagram studies, X-ray powder diffraction, XRD, extended X-ray absorption fine structure spectroscopy, EXAFS and magnetic measurements.

These particular dopants were chosen since, although several studies on Ni- and Co-doped $LiNbO_3$ have been carried out using techniques such as EXAFS[11] and electron-spin resonance, ESR, spectroscopy,[12] the results obtained are contradictory. In particular, the lattice site and valency of the dopant were often differently assigned. The oxidation state of Ni and Co in $LiNbO_3$ was reported to be +I,[13] +II,[14] +III[15] and +II,[16] +III,[17] respectively. The dopants were reported to occupy the Li site but with two different possibilities for the exact lattice position: either the central octahedral site with six similar Ni−O and Co−O bonds or an off-center distorted octahedral site leading to three short and three long Ni−O and Co−O bonds.

Experimental Section

Starting materials were reagent grade Li_2CO_3, Nb_2O_5, Ta_2O_5, CoO, and NiO. These were dried at 300 °C, stored in desiccators, and weighed out to give 3−10 g totals for each reaction mixture. These were ground with an agate mortar and pestle, with added acetone to form a paste, dried and fired in Pt crucibles, initially at 700 °C, 2 h, to expel CO_2, then at 800 and 900 °C for 1 h each, reground, and finally heated at 1000−1250 °C, depending on composition for 24 h. After firing, samples were removed from the furnace, cooled, crushed, and analyzed by XRD using a Philips Hägg Guinier camera, Cu $K\alpha_1$ radiation. To identify the phases present, the films were compared with those of $LiNbO_3$, $LiTaO_3$, possible secondary phases such as $LiNb_3O_8$ or Li_3NbO_4 and starting materials, NiO and CoO. For Rietveld refinement of XRD data, a Stoe Stadi diffractometer incorporating a small, linear position sensitive detector was used: Cu $K\alpha_1$ radiation, data collected over the range 20°−120° 2θ in 0.02° steps with a counting time of 9 s per data point, data analyzed and refined using the Stoe software package suite. During refinement, the unit-cell constants, scale factor, 2θ zero-point, three half-width parameters, five background parameters, lithium and oxygen positional coordinates, and isotropic thermal vibration parameters were varied. EXAFS data were recorded on station 7.1 at the Daresbury Synchrotron radiation source and processed using in-house software.

Results

The ranges of compositions that form single phase solid solutions of Ni,Co in $LiNbO_3$ and $LiTaO_3$ were determined experimentally from an analysis of reaction products obtained on firing samples at 1000−1250 °C.

(10) Villafuerte-Castrejon, M. E.; Aragon-Pina, A.; Valenzuela, R.; West, A. R. *J. Solid State Chem.* **1987**, *71*, 103−108.
(11) Chadwick, A. V. *Solid State Ionics* **1993**, *63*−*65*, 721−727.
(12) Zhou, K.-W.; Zhao, S.-B.; Wu, P.-F.; Xie, J.-K. *Phys. Status Solidi* **1990**, *B162*, 193−198.
(13) Corradi, G.; Polgar, K.; Bugai, A. A.; Zaritskii, I. M.; Grachev, V. G.; Deryugina, N. I. *Sov. Phys. Solid State* **1986**, *28*, 412−417.
(14) Li, Y. *J. Phys. Condens. Matter.* **1995**, *7*, 7075−4080.
(15) Zhao, M. G.; Siu, G. G. *Phys. Rev.* **1995**, *B51*, 6246−6248.
(16) Donnerberg, H. J.; Schirmer, O. F. *Solid State Commun.* **1987**, *63*, 29−32.
(17) Schirmer, O. F.; Thiemann, O.; Wöhlecke, M. *J. Phys. Chem. Solids* **1991**, *52*, 185−200.

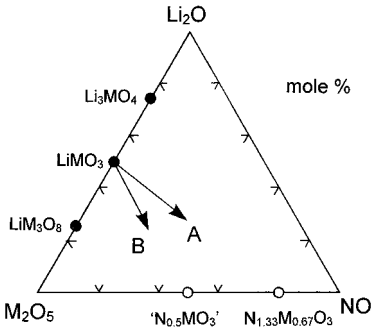

Figure 2. Location of phases in a composition triangle; directions A stoichiometric join, B constant *M* join.

The main technique used to assess whether samples were phase-pure was XRD. For samples that were multiphase after an initial firing for 24 h, a second firing was given at slightly higher temperature.

In carrying out solid state reactions such as these and for phase diagram determination, the approach used was to try and ensure that there was no overall compositional change of the sample during firing. If this were the case, then bulk chemical analysis of the products would not be necessary. For the present materials, the most likely compositional deviations during synthesis involve either lithia loss by volatilization or contamination of the Pt reaction vessels by NiO or CoO or both. Two approaches were used to assess whether these were significant. Neither was entirely satisfactory, but the combined results indicated that final compositions differed by no more than 1−2 mol % of each oxide from the starting compositions.

First, a selection of samples was dissolved in HF and the solutions were analyzed by inductively coupled plasma-atomic emission spectroscopy, ICP-AES; the method was rather unsatisfactory, however, since sometimes, undissolved solid remained after acid treatment. The results showed that lithia contents were often lower than expected, usually by about 1 mol %, for both doped and undoped samples; the discrepancy was generally greater for Ta-based samples than for Nb-based ones, perhaps because somewhat higher final reaction temperatures were used for doped $LiTaO_3$, 1250 °C compared with doped $LiNbO_3$, 1150 °C, leading to a small amount of volatilization of Li_2O. Correspondingly, Ni, Co, Nb, and Ta contents were often slightly high but their ratios, e.g. Nb:Ni, were as expected.

The second method used electron probe microanalysis, EPMA, on mounted, polished sections of sintered pellets. Li cannot be analyzed by EPMA and since the errors associated with direct measurement of O contents of these samples were large, O was not analyzed. Results again showed good agreement between expected and analyzed Co/Ni and Nb/Ta contents at the 1−2 mol % level. It is concluded that, at this level, the final compositions are similar to the starting compositions; there was no evidence of systematic deviation apart from the possibility of a small amount of lithia loss.

The experimentally determined solid solution composition ranges can be represented on a ternary composition triangle of the kind shown in Figure 2. Results for three of the four systems studied are shown on appropriate parts of the ternary composition grids in Figures 3-5. The $LiNbO_3$:Ni solid solution area was determined at five temperatures (Figure 3b) and shows a very marked temperature dependence. At the highest temperature, 1150 °C (Figure 3a) the compositions studied are marked and the nature of the data points indicates whether the products were either single phase solid solution (closed circles) or phase mixtures (open circles). Also shown are the analytical results (squares) on three compositions (large circles) showing reasonably close agreement between expected and analyzed compositions: the data points are not superimposed but are side by side.

The solid solutions form a wedge-shaped area, which extends in the general direction on the phase diagram (Figures 2 and 3) of the composition $Ni_4Nb_2O_9$ (or $Ni_{1.33}Nb_{0.67}O_3$). This means, on comparing the formulas of $LiNbO_3$ (or $Li_3Nb_3O_9$) and $Ni_4Nb_2O_9$, that the main substitution mechanism is $3Li + Nb \rightleftharpoons 4Ni$; crystallographic studies are of course required to determine the site occupancy details of the substitution mechanism. The join $LiMO_3$-"$N_4M_2O_9$", join A in Figure 2, is referred to as the "stoichiometric join" since on it the cation:oxygen ratio remains at 2:3. With increasing Ni content, unit cell parameters (not shown) gradually change from $a \sim 5.140$, $c \sim 13.855$ Å in $LiNbO_3$ to $a \sim 5.140$, $c \sim 13.90$ Å at the Ni-rich solid solution limit, $Li_{0.75}Nb_{0.95}Ni_{0.25}O_3$.

In the $LiTaO_3$:Ni system (Figure 4) the solid solution area also runs roughly parallel to the stoichiometric join, A, with a solid solution limit, 23% NiO comparable to that in the $LiNbO_3$ system. For the two compositions analyzed in this system, the discrepancy between expected and analyzed compositions is significant (Figure 4) but does not lead us to doubt the general validity of the phase diagram results. In the two Co-containing systems, similar solid solution areas form. Results are shown only for the Nb system (Figure 5); the solid solution limit, ~25% CoO, is slightly greater than in the corresponding NiO system, ~23% NiO.

The phase diagrams (Figures 2−5) are presented, for simplicity, in terms of oxide mole percentages as the compositional variable. It is, however, more useful, when considering the stoichiometry ranges and doping mechanisms of the solid solutions, to use a general formula, $Li_{1-5x-3y}M_{1+x-y}N_{4y}O_3$: M = Nb,Ta; N = Ni,Co, in which x and y are the compositional variables. The solid solution areas of the three systems shown in Figures 3−5 are reproduced in Figure 6 but with a compositional grid based on x and y as variables. From this, it is clearly seen that the maximum range of x for undoped materials is $0 < x \leq 0.03$ (but this range reduces at lower temperature) and with increasing dopant content, there is a gradual reduction in the range of x observed. The maximum extent of dopant substitution, y, for each system is given by

$0 < y < 0.065$: M= Nb, N = Ni;
$0 < y < 0.07$: M = Nb, N = Co

$0 < y < 0.060$: M = Ta, N = Ni;
$0 < y < 0.07$: M = Ta, N = Co

At this point, the features of a special line (dashed) through the phase diagrams, corresponding to $x = y$ in the general formula, may be mentioned. This is referred to as the "constant M" join, labeled B, in Figure 2 and has the simplified formula $Li_{1-8y}MN_{4y}O_3$, in which the replacement mechanism $2Li \rightleftharpoons N$ is operative. Simple structural considerations would lead us to expect the

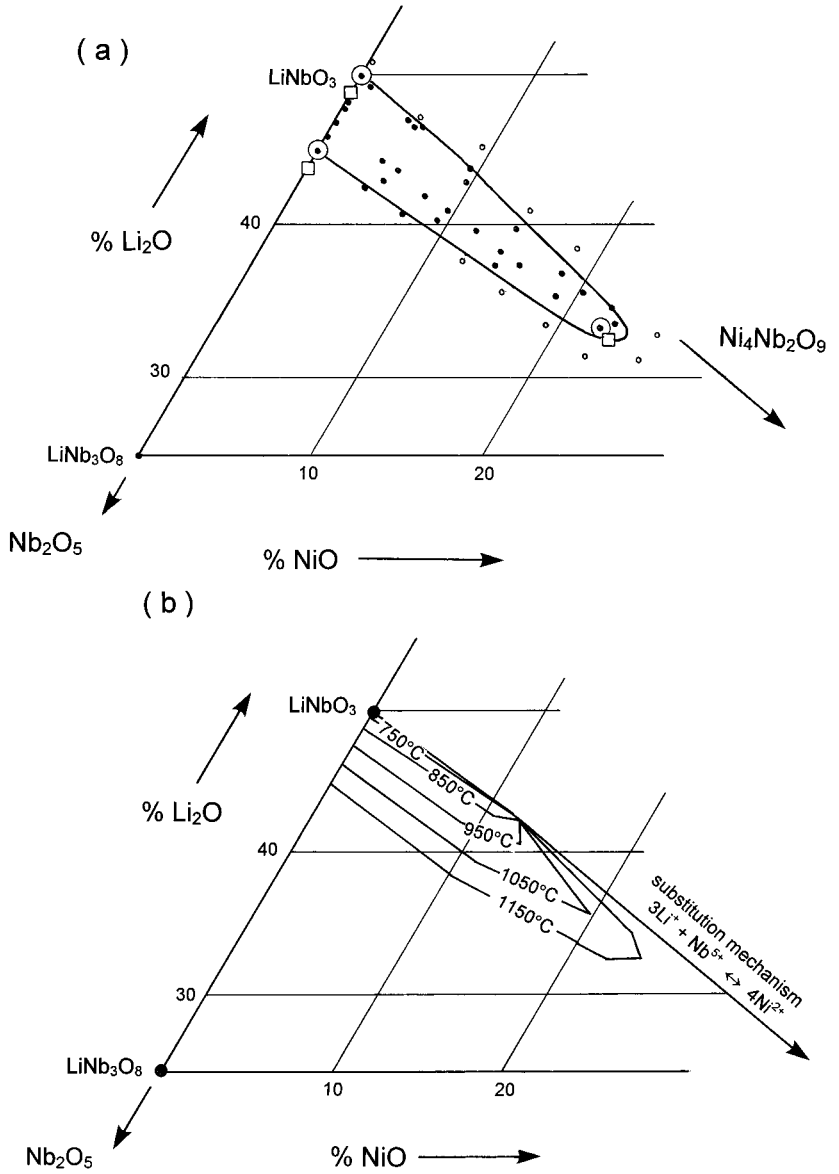

Figure 3. Compositional extent of $LiNbO_3$:Ni solid solutions: (a) at 1150 °C, showing compositions studied; ● single phase product, ○ phase mixtures; and (b) at five temperatures.

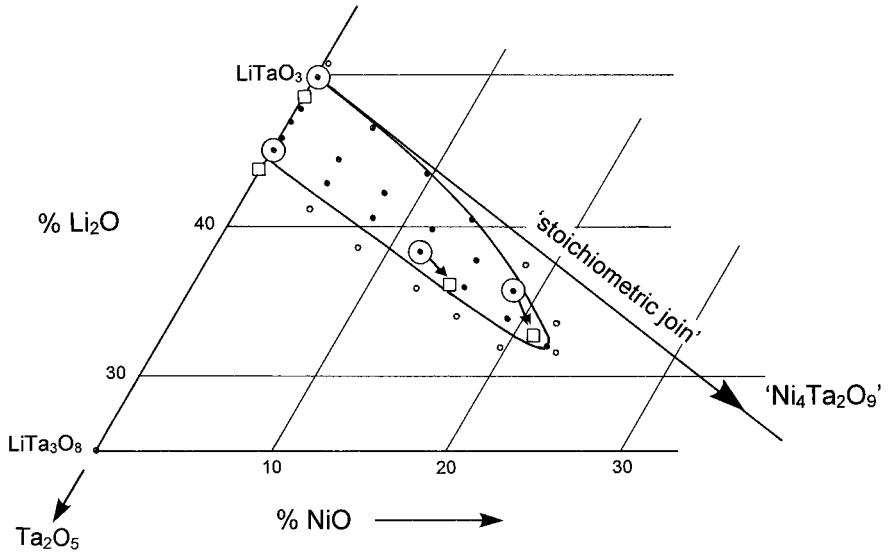

Figure 4. Compositional extent of $LiTaO_3$:Ni solid solutions.

MO_3 lattice to remain intact, N to substitute onto Li sites and the charge difference to be compensated by Li vacancies.

The location of the constant M line, B, effectively divides the solid solution areas into two parts (Figure 6). In region I between the stoichiometric join, A (Figure

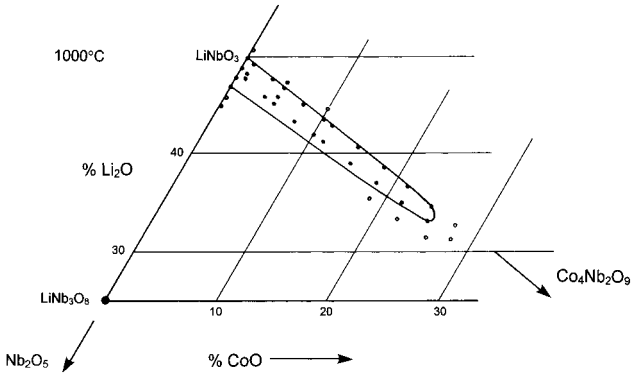

Figure 5. Compositional extent of $LiNbO_3$:Co solid solutions.

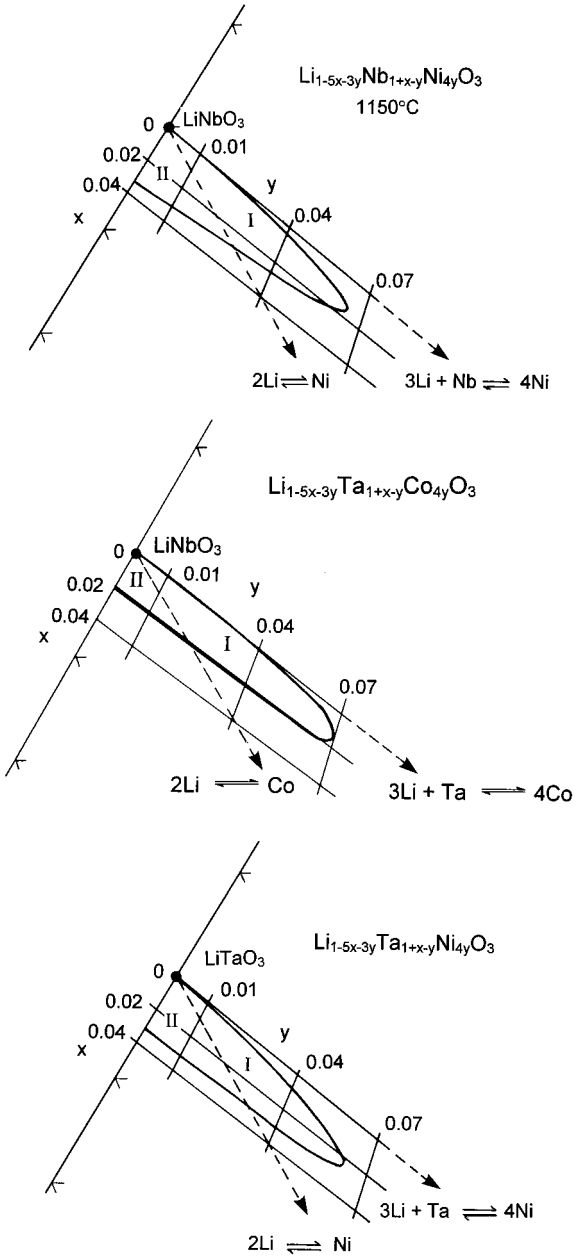

Figure 6. Compositional extents of the solid solutions shown in Figures 3−5 replotted on compositional axes x and y in the general formula $Li_{1-5x-3y}M_{1+x-y}N_{4y}O_3$.

2) and the constant M join, B, there would be insufficient M present for the M sites to be fully occupied by M. By contrast, on the other side of the constant M join, region II, there would be an excess of M and it would be necessary for the spillover to occupy extra sites, presumably the Li sites. Structural studies were therefore carried out to test these hypotheses concerning doping mechanisms that arose from the phase diagram analyses.

Structural studies on a range of solid solutions were carried out by Rietveld refinement of powder XRD data. Starting coordinates of $LiNbO_3$ were used and models with various cation site occupancies were tested. Unique refinement minima could not be obtained for two reasons. First, the decoupling of thermal vibration factors and site occupancies is not generally feasible with laboratory-based XRD equipment. Second, with the possibility of varying amounts of three cations: Li, M, and N, as well as an indeterminate number of cation vacancies, on both the Li sites and the M sites, it was not possible uniquely to determine cation site occupancies.

The following criteria to assess the quality of a particular refinement model were used. First, the values of the reliability indices were used as a guide, with the lowest values taken as an indicator of the most probable structural solution. Often, however, the R factors were fairly insensitive to different models. Second, the thermal vibration factors were used to indicate whether the site distributions for a particular model were appropriate, i.e., whether the effective, average number of electrons in a particular site was realistic. The thermal vibration factor of the lithium site was particularly sensitive to the different models due to the large difference in atomic number of lithium and the other cations. Again, however, there were uncertainties in this approach due to the difficulty in specifying optimum values for the thermal vibration factors in sites with mixed occupancy.

With the above difficulties in mind, partial structure solutions could nevertheless be obtained as illustrated next for one composition taken from region I, $Li_{0.8}Nb_{0.96}Ni_{0.2}O_3$, i.e. $x = 0.01$, $y = 0.05$, Table 1a. Refinements on three models characterized by different cation distributions, are compared.

Model 1: M sites fully occupied by all of the Nb and some of the Ni.

Model 2: M sites fully occupied by Nb and Ni but with some Nb displaced onto Li sites and extra Ni on Nb sites.

Model 3: M sites partially occupied, by Nb only.

Model 3 can be rejected on the grounds that (a) its R factors are significantly higher than for the other models and (b) the thermal vibration factors of the Li sites are too high (associated with the excess of Ni on these sites). Models 1 and 2 are less easy to distinguish. The lithium thermal vibration factor is somewhat lower for model 1 and two of the R factors are slightly lower; model 1 is therefore more likely to be correct than model 2. This means that the Nb sites are fully occupied: all the Nb present in the structure is on the Nb sites and the balance is made up with Ni.

Rietveld refinements similar to these were carried out on a range of compositions falling into regions I and II or on join B. In all cases, the thermal vibration of the lithium site, U_{Li}, was sensitive to the different models and so greater weighting was given to it than to the R factors. A general pattern of behavior was clear. It is

Table 1. Refinement Results Obtained by Powder XRD for $Li_{0.8}Nb_{0.96}Ni_{0.2}O_3$: Comparison of Three Refinement Models and Some Bond Distances (Å)

A. Comparison of the Three Models

model[a]	I $[Li_{0.8}Ni_{0.16}]$ $[Nb_{0.96}Ni_{0.04}]O_3$	II $[Li_{0.8}Ni_{0.15}Nb_{0.01}]$ $[Nb_{0.95}Ni_{0.05}]O_3$	III $[Li_{0.8}Ni_{0.2}]$ $[Nb_{0.96}]O_3$
$O(Li_{Li})$	0.8	0.8	0.8
$O(Ni_{Li})$	0.16	0.15	0.2
$O(Nb_{Li})$		0.01	
$O(Nb_{Nb})$	0.96	0.95	0.96
$O(Ni_{Nb})$	0.04	0.05	
a (Å)	5.1425(1)	5.1425(1)	5.1425(1)
c (Å)	13.8948(4)	13.8948(4)	13.8948(4)
z(Li)	0.290(1)	0.290(1)	0.292(1)
x(O)	0.046(2)	0.046(2)	0.047(2)
y(O)	0.343(4)	0.343(4)	0.344(4)
z(O)	0.064(1)	0.064(1)	0.065(1)
U_{Li} (Å^2)	0.027(6)	0.031(6)	0.059(7)
U_{Nb} (Å^2)	0.007(1)	0.007(1)	0.008(1)
U_O (Å^2)	0.007(3)	0.008(3)	0.010(3)
R_p (%)	6.65	6.65	6.80
R_{wp} (%)	9.05	9.06	9.25
R_I (%)	4.64	4.74	5.63

B. Bond Distances in $LiNbO_3$ and Derivatives

composition	Li−O(3×)	Li−O(3×)	Nb−O(3×)	Nb−O(3×)
$LiNbO_3$ stoichiometric	2.050	2.271	1.876	2.130
$Li_{0.95}Nb_{1.01}O_3$ congruent	2.053	2.274	1.879	2.126
$Li_{0.8735}Nb_{1.0253}O_3$ highly nonstoichiometric	2.039	2.277	1.900	2.116
$Li_{0.8}Nb_{0.96}Ni_{0.2}O_3$ congruent:Ni-doped	2.095	2.172	1.882	2.128
$Li_{0.74}Nb_{0.94}Co_{0.28}O_3$ congruent:Co-doped	2.102	2.279	1.795	2.189

[a] $O(Li_{Li})$, *etc.*, refers to the occupancy of Li sites by Li.

convenient to commence with join B since results for it were the simplest.

On join B, it is clear that M sites are fully and exclusively occupied by Nb,Ta; vacancies associated with the solid solution mechanism are located entirely on the Li sites. This conclusion is supported by the study of a similar model for Mg-doped $LiNbO_3$, $Li_{1-2x}Mg_{2x}NbO_3$, by Thomson et al.[18]

In region I, there is a deficiency of Nb/Ta compared with join B and an excess of both Li and Ni/Co. Refinement results indicate that the M sites are fully occupied, with all the available Nb/Ta cations and sufficient Ni/Co to achieve full occupancy. Vacancies are again concentrated on Li sites. In region II, by contrast, there is an excess of Nb/Ta compared with join B; this excess spills over to occupy the Li sites, together with Li, Ni/Co and vacancies.

The Rietveld refinements give information on net site occupancies and, from the atomic coordinates, the average site geometries (bond distances, angles) can be calculated. Thus, the Li site geometry is an average of that of the Li, Ni/Co, and Nb/Ta occupants; these may have either identical geometries or rather different geometries which are averaged in the refinement. Similarly, the Nb/Ta site is an average of that of Nb/Ta and Ni/Co occupants. The results show that the octahedra associated with both Nb/Ta and Li sites are distorted (Table 1b): this is because cation repulsions in the z direction between the two sets of sites which share a common face of three oxygens cause an off-center, antiparallel displacement within the octahedra (Figure 1a). Consequently, the six metal−oxygen distances of each octahedron split into two groups of three distances (Table 1b). For a range of doped and undoped lithium niobates, bond distances varied little with composition.

To investigate the local site geometries in more detail, especially the geometry of the Ni/Co environments, EXAFS measurements on selected samples were made. Normalized and Fourier-transformed spectra of the Ni and Co K edges in doped, congruently melting $LiNbO_3$ are shown in Figure 7. The structural parameters obtained by fitting to these spectra and those of other compositions are listed in Table 2.

The spectra show two broadened peaks with their maxima around 2.1 and 3.2 Å. The first peak is fitted by a composite of two peaks, each representing three Ni/Co−O distances. This shows clearly that Ni and Co are located off-center in octahedral sites with three short and three long bonds to oxygen and is similar to the XRD refinement results, although those data gave averaged site coordination geometries rather than ion-specific geometries. The Li sites share a common face with NbO_6 octahedra (Figure 1a), and cation repulsions are responsible for the off-center displacement.

The second peak is also a composite of two main peaks, each representing three next nearest neighbor Ni/Co−Nb distances. Additional peaks associated with Ni/Co−next nearest neighbor oxygen atoms are also present but of low intensity. The occurrence of the second peak is strong evidence that a significant fraction of Ni/Co occupy the Li sites in the crystal structure of $LiNbO_3$, rather than the Nb sites or the vacant octahedral sites. If, instead, Ni/Co were located exclusively on the Nb sites, then no Nb neighbors at a distance of ∼3.2 Å would be expected and this peak should be absent from the EXAFS spectrum. A small concentration of Ni/Co on the Nb sites is, of course, expected for

(18) Thomson, J. B.; Small, C.; Lightfoot, P.; Bruce, P. G. *J. Mater. Chem.* **1995**, *5*, 1039−1041.

(19) Goodenough, J. B. *Magnetism and the Chemical Bond*; John Wiley & Sons: New York, 1963; pp 98−109.

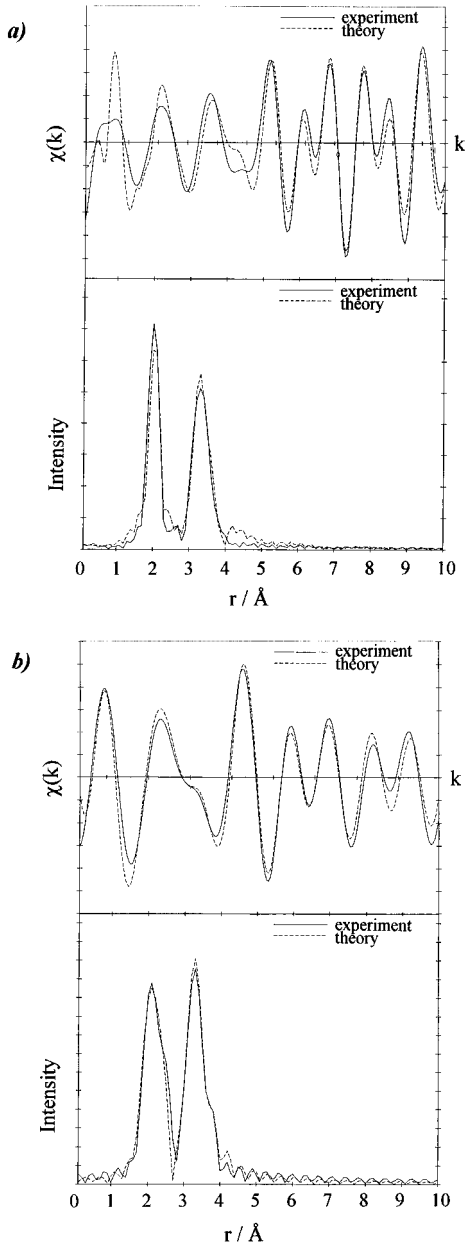

Figure 7. Normalized EXAFS spectra (above) and Fourier transform (below) of the K edge in (a) $Li_{0.875}Nb_{0.985}Ni_{0.1}O_3$ and (b) $Li_{0.8}Nb_{0.96}Co_{0.2}O_3$.

Table 2. Fitted Parameters to the Ni/Co K-edge EXAFS of Doped Li(Nb/Ta)O_3 with Ni/Co Located in Li Positions[a]

shell	atom type	coordn no.	*x*, *y*	bond distance (Å)	Debye−Waller factor (Å^2)
			(a) $Li_{1-5x-3y}Nb_{1+x-y}Ni_{4y}O_3$		
1	O	3.0	0.01, 0.00	2.049	
			0.01, 0.0125	2.057(5)	0.004(1)
			0.01, 0.025	2.104(3)	0.000(1)
2	O	3.0	0.01, 0.00	2.272	
			0.01, 0.0125	2.20(1)	0.018(3)
			0.01, 0.025	2.34(2)	0.035(9)
3	Nb	4.0	0.01, 0.00	3.067	
			0.01, 0.0125	3.187(8)	0.012(2)
			0.01, 0.025	3.24(1)	0.012(4)
4	O	3.0	0.01, 0.00	3.282	
			0.01, 0.0125	3.32(6)	0.004(6)
			0.01, 0.025	3.30(2)	0.001(9)
5	Nb	3.0	0.01, 0.00	3.353	
			0.01, 0.0125	3.43(12)	0.021(4)
			0.01, 0.025	3.52(3)	0.022(8)
6	O	3.0	0.01, 0.00	3.413	
			0.01, 0.0125	3.36(10)	0.024(2)
			0.01, 0.025	3.54(3)	0.002(6)
			(b) $Li_{1-5x-3y}Ta_{1+x-y}Co_{4y}O_3$		
1	O	3.0	0.01, 0.02	2.000(4)	0.009(1)
			0.00, 0.04	2.070(5)	0.009(1)
			0.00, 0.05	2.000(5)	0.017(1)
			0.01, 0.05	2.014	0.018
			0.00, 0.06	2.029(2)	0.012(3)
			0.01, 0.07	2.036(2)	0.013(1)
2	O	3.0	0.01, 0.02	2.350(15)	0.028(5)
			0.00, 0.04	2.423(9)	0.020(4)
			0.00, 0.05	2.450(9)	0.026(3)
			0.01, 0.05	2.462	0.006
			0.00, 0.06	2.424(4)	0.021(1)
			0.01, 0.07	2.415(4)	0.023(1)
3	Ta	4.0	0.01, 0.02	3.063(27)	0.020(5)
			0.00, 0.04	3.163(13)	0.005(2)
			0.00, 0.05	3.097(9)	0.005(2)
			0.01, 0.05	3.080	0.002
			0.00, 0.06	3.167(7)	0.003(2)
			0.01, 0.07	3.204(5)	0.008(1)
			(c) $Li_{0.68}TaNi_{0.16}O_3$, $x = 0.04$, $y = 0.04$		
1	O	3.0		2.096(3)	0.004(1)
2	O	3.0		2.517(7)	0.028(4)
3	Ta	4.0		3.031(16)	0.015(2)
			(d) $Li_{0.8}Nb_{0.96}Co_{0.2}O_3$, $x = 0.01$, $y = 0.05$		
1	O	3.0		2.066(3)	0.015(1)
2	O	3.0		2.491(3)	0.021(1)
3	Nb	4.0		3.095(4)	0.023(1)

[a] The coordination numbers were held constant during the refinement.

compositions in region I (Figure 6).

The antiparallel displacement of atoms in face-sharing Li and Nb/Ta sites, Figure 1a, leads to an equalization of cation−cation distances in what otherwise would be separate nearest and next-nearest distances. Within the close-packed layers, Figure 1b, a Li site (white circle) is surrounded by three Nb sites (small black circles) and three octahedral vacancies forming, ideally, a coplanar arrangement. The Li site also has a single close Nb neighbor across a shared octahedral face in a direction perpendicular to the coplanar arrangement (Figure 1a). Due to the antiparallel cation displacements, the Li−Nb distance across the shared octahedral face (Figure 1a) is found to be essentially the same as the three coplanar Li−Nb distances (Figure 1b). For this reason, it was convenient to consider these four Nb atoms as a single group in the EXAFS refinements (Table 2).

The Ni−O, Co−O distances obtained from refinement of the EXAFS data (Table 2) are comparable to Li−O distances in undoped and doped $LiNbO_3$ obtained from crystal structure refinements (Table 1b) and the octahedra show similar trigonal distortions. This is consistent with the similarity in ionic radii and, therefore, bond lengths to oxygen of Li^+, Ni^{2+}, and Co^{2+}. In the case of Co-doped $LiTaO_3$ for which EXAFS data on several compositions were obtained (Table 2) there is no noticeable, systematic variation in bond lengths with composition. The similarity in EXAFS-derived bond lengths for Co,Ni−O to those of XRD-derived bond lengths for the Li−O site rather than the Nb,Ta−O site is further evidence that Co,Ni occupy, primarily, the Li site.

Thus far, the phase diagram, X-ray diffraction, and EXAFS results have given a variety of information leading to a clear picture of the solid solution mechanisms and defect structures in Ni/Co-doped $LiNbO_3$ and $LiTaO_3$. The basic assumption throughout has been that Ni and Co are present as divalent cations. Evi-

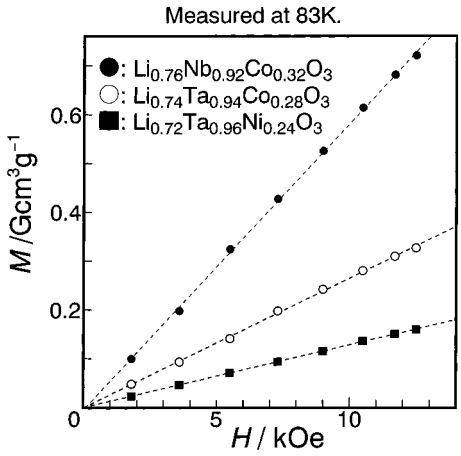

Figure 8. Field dependence of magnetization, M, at 83 K. Broken straight lines are fits to the data between 1.8 and 12.5 kOe.

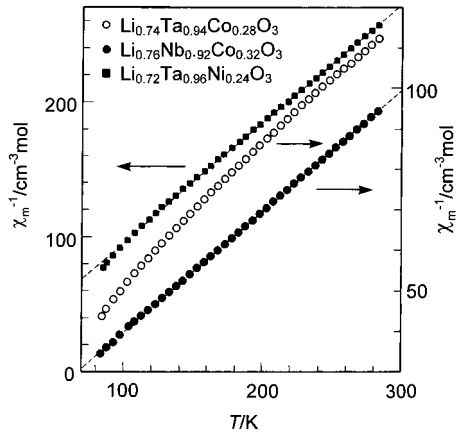

Figure 9. Temperature dependence of inverse molar susceptibility (χ_m^{-1}) between 83 and 290 K. Broken straight lines are fits to the data above 100 K. Applied magnetic fields were 9 kOe for $Li_{0.72}Ta_{0.96}Ni_{0.24}O_3$ and 11.7 kOe for the other samples.

dence to confirm the charge state of the cations was sought from magnetic measurements over a range of temperatures (4−300 K).

Three compositions with high dopant contents—$Li_{0.76}Nb_{0.92}Co_{0.32}O_3$, $Li_{0.74}Ta_{0.94}Co_{0.28}O_3$ and $Li_{0.72}Ta_{0.96}Ni_{0.24}O_3$—were studied. All fall into regions I of the phase diagrams (Figure 6). The dependence of the magnetization, M, on magnetic field, H, at 83 K is shown in Figure 8. For each, the data fitted a straight line with zero intercept, thus indicating the absence of any spontaneous magnetization for $T \geq 83$ K.

The temperature dependence of the inverse molar magnetic susceptibilities, χ_m^{-1}, between 83 and 290K is shown in Figure 9. Two samples showed linear, Curie−Weiss paramagnetic behavior down to 100 K but the third, $Li_{0.74}Ta_{0.94}Co_{0.28}O_3$, showed linear dependence only above ~160 K. The Curie−Weiss law, [$\chi_m^{-1} = (T - \theta)/C_m$, $\mu_{eff}/\mu_B = (3kC_m/N\mu_B^2)^{1/2}$; C_m, Curie constant; k, Boltzmann constant; N, Avogadro's number] was applied to each χ_m^{-1} vs T data set. Calculated effective magnetic moments, μ_{eff} per Co/Ni and Weiss temperatures, θ, are summarized in Table 3, together with typical literature values for these ions.

The μ_{eff} values for all three samples are typical of the high spin, divalent state, $t_{2g}^5 e_g^2$ (Co^{2+}) and $t_{2g}^6 e_g^2$ (Ni^{2+}). The reason for the deviation from Curie−Weiss behavior below 160 K for Co-doped $LiTaO_3$, but not for Co-doped $LiNbO_3$ is not clear. The former sample was purple and the latter black, which may indicate the possibility of some mixed valence in the Co-doped $LiNbO_3$ sample.

Table 3. Calculated Effective Magnetic Moments, μ_{eff}, and Weiss Temperature, θ, for Three Doped Samples[a]

composition	μ_{eff}/μ_B	θ/K	typical μ_{eff} values[18]
$Li_{0.76}Nb_{0.92}Co_{0.32}O_3$	5.172(3)	−32.5(5)	5.26 μ_B ($CoCl_2$), 5.13 μ_B (CoF_2)
$Li_{0.74}Ta_{0.94}Co_{0.28}O_3$[b]	4.91(2)	−59(3)	
$Li_{0.72}Ta_{0.96}Ni_{0.24}O_3$	2.999(9)	−7(2)	3.5 μ_B (NiF_2), 3.3 μ_B ($NiCl_2$)

[a] The data were obtained by applying a Curie−Weiss law to each of the χ_m^{-1} vs T plots above 100 (or 160) K. [b] The χ_m^{-1} vs T plot deviates from linearity below 160 K (Figure 9).

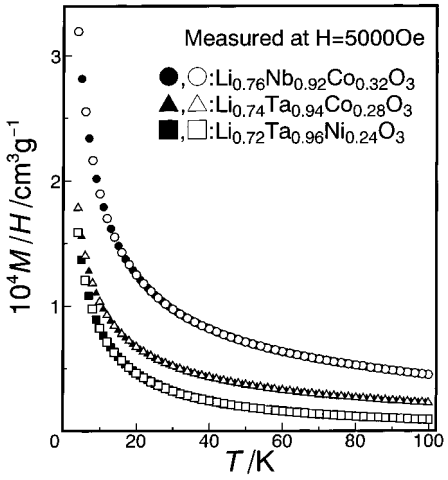

Figure 10. Temperature dependence of normalized magnetization (M/H) between 4 and 100 K. Open data points obtained on field-cooling cycle; closed data points on zero-field cooling cycle.

The large differences in Weiss temperature (Table 3) indicate the possibility of a much stronger magnetic interaction between Co^{2+} ions than between Ni^{2+} ions; in particular, magnetic coupling between Co^{2+} ions below 83 K may occur. Additional measurements below 100 K were therefore made using a SQUID magnetometer. The temperature dependence of the normalized magnetization, M/H, is shown in Figure 10 and is typical of paramagnetic solids. Rapid increases in M/H occur below 10 K, however, and so the field dependence of μ_M at 4 K was investigated (Figure 11). No hysteresis was observed for any of the μ_M/H loops; the high-field data, 7−10 kOe, extrapolated to small positive values of between 0.023 and 0.038μ_B for zero field, indicating a weak coupling between the magnetic ions. This is not attributable to the possible presence of oxide impurity since NiO and CoO show antiferromagnetic spin order below 520 and 291K, respectively, and Co_3O_4 is ferrimagnetic below a Curie temperature of 33 K. The occurrence of magnetic coupling must be associated with the crystallographic arrangement of the Ni^{2+}/Co^{2+} ions which, for these compositions, partially occupy both Li and Nb/Ta sites in the structure of doped $Li(Nb/Ta)O_3$. Thus, the shortest distance between Ni^{2+}/Co^{2+} cations located on adjacent Li and Nb/Ta sites is only ~3 Å. The spontaneous magnetic moments are small, however, and further systematic study as a function of dopant content and site occupancy distribution, at higher fields than currently available to us (10 kOe), is required to

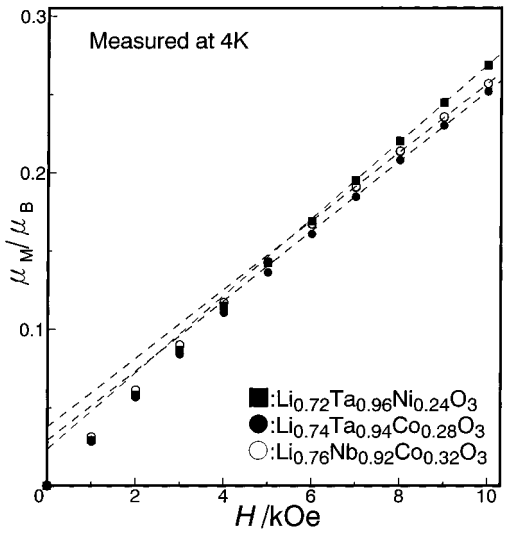

Figure 11. Field dependence of magnetic moment per Co or Ni ion, μ_M at 4 K between 0 and 10 kOe. Broken straight lines are fits between 7 and 10 kOe.

elucidate the nature of the magnetic interactions.

Conclusions

The mechanisms of doping $LiNbO_3$ and $LiTaO_3$ with Ni and Co have been determined. Under the heating conditions used, ~1100−1250 °C in air, magnetic data indicate that the dopants are present as divalent cations. EXAFS data indicate a trigonally distorted octahedral environment for the dopants with three short and three long bonds to oxygen. From the occurrence of an intense first nearest neighbor cation peak, a large fraction of the dopants must be substituted onto Li sites with Nb/Ta as nearest cation neighbors. The trigonal distortion is associated with the sharing of $(Ni/Co)O_6$−$(Nb/Ta)O_6$ octahedra across a common face, which causes a cation−cation repulsion and antiparallel displacement of cations in the z direction of the crystal structure. Depending on composition, some Ni/Co dopants also occupy Nb/Ta sites. Many doped compositions contain less cations than given by the 2:3 cation: oxygen stoichiometry; the cation vacancies are associated exclusively with lithium sites.

One reason there is no apparent consistency in the literature concerning the defect structures of doped $LiNbO_3$ and $LiTaO_3$ is that the structure is very composition-dependent. Thus even in the absence of dopants, both $LiNbO_3$ and $LiTaO_3$ can have variable composition in which excess Nb/Ta substitutes onto Li sites, together with creation of Li site vacancies to maintain charge balance. In Ni/Co-doped materials, two simple extreme doping mechanisms have been identified and these, combined with the substitution of Li by Nb/Ta in undoped materials, provide a framework with which to analyze and interpret the general structural and compositional characteristics of doped materials. These two extreme doping mechanisms are as follows:

First, on the "stoichiometric join" in the compositional phase diagram, Li_2O−$(Nb/Ta)_2O_5$−(Ni/Co)O, the cation:oxygen ratio is maintained constant by means of the complex substitution mechanism $3Li + Nb/Ta \rightleftharpoons 4Ni/Co$. The locus of the solid solution compositional area on the phase diagram shows that this mechanism is the most important and most extensive. This mechanism applies to both stoichiometric $Li(Nb/Ta)O_3$ and to non-stoichiometric, Nb/Ta-rich material and, indeed, the phase diagram results indicate that the solid solutions may be most extensive for the doping of nonstoichiometric $Li(Nb,Ta)O_3$. Phase diagram studies on other doped $Li(Nb/Ta)O_3$ systems, e.g. with Ti^{4+}, indicate that a similar mechanism associated with a stoichiometric join is the main doping mechanism.[10]

Second, on the "constant Nb/Ta" join in the phase diagrams, the Nb/Ta sites remain fully occupied by Nb/Ta and substitution of Ni/Co occurs exclusively on the Li sites, with the simple mechanism $2Li \rightleftharpoons Ni/Co$; clearly, Li site vacancies are created at the same time. The locus of this constant Nb/Ta join in the phase diagrams, line B in Figures 2−6, indicates that this join has no special significance as a doping mechanism; it is simply one direction that passes through the solid solution areas, but is not particularly extensive and has no special characteristics. Despite this, there is a crystallographic simplicity to this mechanism which has been highlighted in studies of Mg-doped $LiNbO_3$.[18]

Although the "constant Nb/Ta" mechanism appears not to be of special significance in evaluating the main doping mechanism, it is significant in dividing the doped materials into two regions, each with a characteristic defect structure. In region I, there is insufficient Nb/Ta to fully occupy their own sites and the deficit is made up of Ni/Co; the lithium sites contain a mixture of Li, Ni/Co, and vacancies. In region II, the Nb/Ta sites are fully occupied by Nb/Ta; the lithium sites contain all the disorder and compositional variation and, in general, contain a mixture of Li, Ni/Co, Nb/Ta, and vacancies.

Acknowledgment. We thank Johnson-Matthey for partial funding of this project, A. M. Coats for EPMA, and G. J. Pugh for the ICP analyses, and EPSRC, Daresbury Laboratory, for EXAFS beamtime.

CM970511T